

Training behavior of deep neural network in frequency domain[★]

Zhiqin John Xu^{1,2}[0000–0003–0627–3520], Yaoyu Zhang^{1,2}, and Yanyang Xiao^{1,2}

¹ New York University Abu Dhabi, Abu Dhabi 129188, United Arab Emirates

² Courant Institute of Mathematical Sciences, 10012, New York University, New York, 10012, NY, United States
zhiqinxu@nyu.edu

Abstract. Why deep neural networks (DNNs) capable of overfitting often generalize well in practice is a mystery in deep learning. Existing works indicate that this observation holds for both complicated real datasets and simple dataset of one-dimensional (1-d) functions. In this work, for fitting classification problems, memorizing natural images and low-frequency dominant 1-d functions, we empirically found that a DNN, e.g., full-connected DNN or convolutional neural network, with common settings first quickly captures the dominant low-frequency components, and then relatively slowly captures high-frequency ones. We call this phenomenon Frequency Principle (F-Principle). F-Principle can be observed over various DNN setups of different activation functions, layer structures and training algorithms in our experiments. F-Principle can shed light on why DNNs often generalize well albeit its ability of overfitting. This F-Principle potentially can provide insights into understanding the general principle underlying DNN optimization and generalization for real datasets.

Keywords: Deep learning · Fourier analysis · Generalization.

1 Introduction

Although Deep Neural Networks (DNNs) is totally transparent, i.e., the value of each node and the strength of each connection can be easily obtained, it is difficult to interpret how information is processed through DNNs. We can easily record the trajectories of the parameters of DNNs during training. However, it is very difficult to understand the principle underlying the highly non-convex problem of DNN optimization [9]. Therefore, albeit its transparency, the DNN is often criticized for being a “black box” [1,16]. Even for the simple problem of fitting one-dimensional (1-d) functions, the training process of the DNN is still not well understood [14,17]. For example, Wu et al. (2017) [17] used DNNs with a different number of layers to fit a few data points sampled from a 1-d function of the third-order polynomial. They found that even when a DNN is capable of over-fitting, i.e., the number of its parameters is much larger than the size of the

[★] Supported by the NYU Abu Dhabi Institute G1301.

training set, it generalizes well (i.e., no overfitting) when it is well trained on the training set. In practice, DNNs often generalize well empirically for much more complicated datasets even when it is capable of over-fitting [7,11,21,20,10,17]. Intuitively, when a network is capable of over-fitting, its solution of optimization lies in a huge space where well-generalized solutions only occupy a small subset. Therefore, it is mysterious that DNN optimization can often lead to a well-generalized solution while ignoring a huge space of over-fitting solutions. To understand the underlying mechanism, in this work, we analyze in detail the principle underlying the DNN optimization process using a class of image classification datasets (MNIST and CIFAR-10), natural images and 1-d functions. Our work could potentially provide insights into how DNNs behave in general during the training and why it tends to a solution of good generalization performance after training.

We empirically found that, for real datasets and synthetic functions, DNNs with common settings first quickly capture the dominant low-frequency components while keeping high-frequency ones small, and then relatively slowly captures those high-frequency components. We call this phenomenon *Frequency Principle*³ (F-Principle). From our numerical experiments, this F-Principle can be widely observed over different neuron numbers (tens to thousands in each layer), layer numbers (one to tens), training algorithms (gradient descent, stochastic gradient descent, Adam) and activation functions (tanh and ReLU). According to F-Principle, DNNs naturally utilize a strategy that is also adopted in some numerical algorithms to achieve remarkable efficiency, namely, fitting the target function progressively in ascending frequency order. These numerical algorithms include, for examples, the Multigrid method for solving large-scale partial differential equations [5] and a recent numerical scheme that efficiently fits the three-dimensional structure of proteins and protein complexes from noisy two-dimensional images [3].

Using F-Principle, we can provide insights into why DNNs often generalize well empirically albeit its ability of over-fitting [7,11,21,20,10,17]. For a finite-size training set, there exists an effective frequency range [15,19,12] beyond which the information of the signal is lost. By F-Principle, with no constraint on the high-frequency components beyond the effective frequency range, DNNs tend to keep them small. For a wide class of low-frequency dominant natural signals (e.g., image and sound), this tendency coincides with their behavior of decaying power at high frequencies. Thus, DNNs often generalize well in practice. F-Principle indicates that the important frequency components of the DNN output are determined by the training data, thus, provides a possible mechanism to understand why DNNs can memorize datasets with random labels but also possess good generalization ability for real datasets [20]. When the training data is noisy, the small-amplitude high-frequency components are easier to be contaminated. By F-Principle, DNNs first capture the less noisy dominant frequency components of the training data and keeps other frequency components small. At this

³ Based on the study of this paper, we develop a theoretical framework to understand F-Principle in [18].

stage, although the loss function is not best optimized for the training data, DNNs could have better generalization performance for not fitting the noise in the higher-frequency components. Therefore, as widely observed, better generalization performance often can be achieved with early-stopping. Empirically, we show that F-Principle helps DNN generalization. Since lower-frequency functions have less complexity, our analysis shows that over-parameterized DNNs tend to fit target functions with low complexity, which is consistent with other studies [17,2]. Lower-frequency functions also have smaller Lipschitz constants. According to the study [6], which focuses on the relation between stability and generalization, smaller Lipschitz constants leads to smaller generalization error.

2 F-Principle in real datasets

In this section, we study the behavior of training process of DNNs in the frequency domain using real datasets. We empirically found that, for a general class of functions dominated by low-frequency components, the training process of DNNs follows the F-Principle in which low-frequency components are first captured, followed by high-frequency components.

2.1 MNIST/CIFAR10

Since the computational cost of high-dimensional Fourier transform is very high, to verify the F-Principle in the image classification problems (MNIST and CIFAR-10), we perform the Fourier analysis in the first principle component of the input space. The procedure is as follows.

The training set is a list of images with labels: $\{\mathbf{x}_k, y_k\}_{k=0}^{n-1}$. Each image is represented by a vector $\mathbf{x}_k \in \mathbb{R}^{N_{in}}$, where N_{in} is the pixel number of an image. $y_k \in \mathbb{R}$ is the label. We use two DNN structures to learn this training set, that is, a full-connected DNN and a CNN. In both structures, the dimensions for the input layer and the output layer are N_{in} and 1, respectively.

First, we compute the first principle direction. Translate each image by

$$\mathbf{x}'_j = \mathbf{x}_j - \frac{1}{n} \sum_{k=0}^{n-1} \mathbf{x}_k, \quad j = 0, 1, \dots, n-1.$$

Denote all images by $X = [\mathbf{x}'_0, \mathbf{x}'_1, \dots, \mathbf{x}'_{n-1}] \in \mathbb{R}^{N_{in} \times n}$. The covariance matrix is $C_x = XX^T$. The eigenvector of the maximal eigenvalue of C_x can be obtained, denoted by $\mathbf{p}_1 \in \mathbb{R}^{N_{in}}$, i.e., the first principle direction. The projection of each image in the \mathbf{p}_1 direction is $x'_k \triangleq \mathbf{p}_1^T \mathbf{x}_k$. We rescale x'_k to x_k such that $x_k \in [0, 1]$ by

$$x_k = \frac{(x'_k - \min_j x'_j)}{\max_l (x'_l - \min_j x'_j)}.$$

Then, the sample set is $S = \{(x_k, y_k)\}_{k=0}^{n-1}$. Note that now $\{x_k\}_{k=0}^{n-1}$ is a non-uniform sampling. Using non-uniform FFT (NUFFT), we can obtain

$$F[f][\gamma_k] = \sum_{j=0}^{n-1} y_j \exp(-2\pi i x_j k).$$

Then, the sampling on the Fourier domain is $S_\gamma = \{(\gamma_k, F[f](\gamma_k))\}_{k=0}^{n-1}$. After each training step, we feed each \mathbf{x}_k into the DNN and obtain the DNN output $T(\mathbf{x}_k)$: $S_T = \{(x_k, T(\mathbf{x}_k))\}_{k=0}^{n-1}$. Using non-uniform FFT (NUFFT), we can obtain the sampling of the DNN on the Fourier domain is $S_{T,\gamma} = \{(\gamma_k, F[T](\gamma_k))\}_{k=0}^{n-1}$. To examine the convergence behavior of different frequency components during the training of a DNN, we compute the relative difference of the DNN output and $f(x)$ in frequency domain at each recording step, i.e.,

$$\Delta_F(\gamma) = \frac{|F[f](\gamma) - F[T](\gamma)|}{|F[f](\gamma)|}, \quad (1)$$

where T denotes the DNN output. We perform the experiments on two dataset, i.e., MNIST and CIFAR-10. Due to the computational cost, we use the test samples of both datasets to train the neural networks. As shown in the first column in Fig.1, both two datasets have clear dominant low-frequency components in the first principle direction. By examining the relative error of certain selected important frequency components (marked by black squares), we can see that except for few components, the DNNs capture the training data from low to high frequency, that is, the F-Principle holds very well in both datasets and both network structures (second and third column in Fig.1).

2.2 Natural images

To show the F-Principle holds in real data and helps generalization, we train a DNN to fit a natural image (a mapping from position (x, y) to gray scale strength). As an illustration of F-Principle, we study the Discrete Fourier Transform (DFT) of the image with respect to x for a fixed y (red dashed line in Fig.2a). Note that because the frequency in DFT is discrete, we can refer to a frequency component by its index instead of its physical frequency. The Fourier coefficient of $f(x)$ for the γ -th frequency component is denoted by $F[f](\gamma)$ (a complex number in general). $|F[f](\gamma)|$ is the corresponding amplitude, where $|\cdot|$ denotes the absolute value. Note that we call γ the *frequency index*. We observe that, F-Principle holds for small initialization (a common setting) as shown in Fig.2b and 2c. However, F-Principle fails for large initialization (Fig.2d). When F-Principle applies, DNN captures the image from coarse-grained low-frequency components to detailed high-frequency components (Fig.2e-2g) and generalizes well (Fig.2h). When F-Principle fails, the DNN output is very noisy (Fig.2i-2k) and generalizes poorly (Fig.2l).

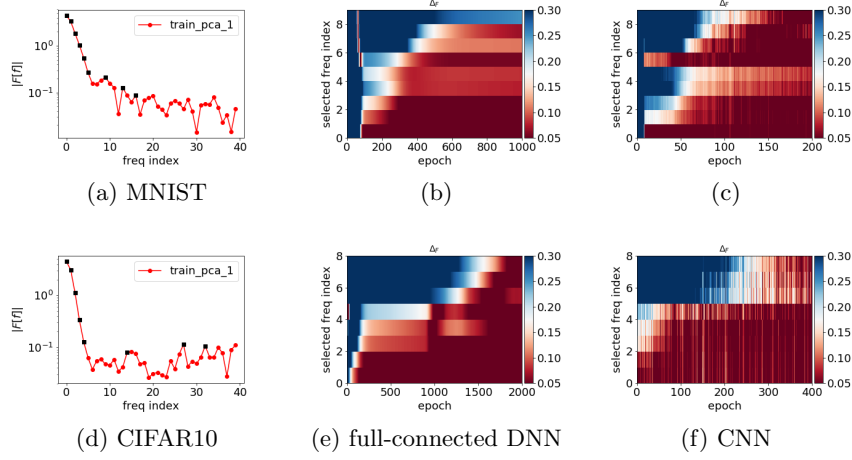


Fig. 1: Frequency analysis of the first principle component. The training datasets for the first and the second row are from MNIST and CIFAR10, respectively. The neural networks for the second column and the third column are full-connected DNN and CNN, respectively. (a,d) $|F[f]|$ at the direction of the first principle component. The selected components are marked by black dots. (b, c, e, f) Δ_F at different recording epochs for different selected frequency. Δ_F larger than 0.3 (or smaller than 0.05) is represented by blue (or red). full-connected DNN setup: width 200-100-100; activation: tanh; batch size: 100; learning rate: 10^{-5} for CIFAR10 and 10^{-6} for MNIST; Gaussian initialization with mean 0 and standard deviation 10^{-4} . CNN setup: two layers of 32 features with 3×3 convolutional kernel and 2×2 max-pooling, followed by 128-64 dense networks; activation: relu; batch size: 128; learning rate: 10^{-4} for CIFAR10 and 10^{-5} for MNIST; Gaussian initialization with mean 0 and standard deviation 0.05.

3 Analysis of the F-Principle

In this section, we will use synthetic data to study the F-Principle. The advantage of the synthetic data is that it can preserve the F-Principle found in the real datasets, and also simple enough to perform more analysis.

3.1 F-Principle in synthetic data

Natural signals (e.g., image and sound) generally have large power at low frequencies and decreasing power at high frequencies [4]. This observation motivates us to design a class of functions with dominant low-frequency components to study the behavior of training process of DNNs. Especially, we are interested in how and when each frequency component is captured during the training of DNNs. We design a target function by discretizing a smooth function $f_0(x)$ as

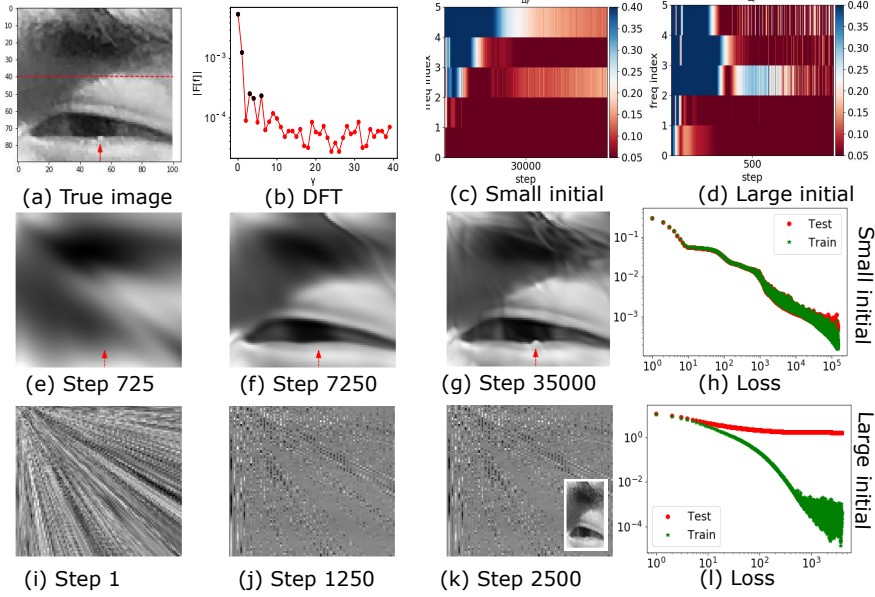


Fig. 2: Fitting a natural image. The training data are all pixels whose horizontal indexes are odd. (a) True image, an eye. (b) $|F[f]|$ of the red dashed pixels in (a) as a function of frequency index with important peaks marked by black dots. (c,d) Δ_F at different recording steps for different selected frequency peaks. The standard deviations of the initialization for the second and the third row are 0.01 and 0.5, respectively. (e-g, i-k) DNN outputs at different steps. The inset in (k) is the DNN's output at Step 2500 on training pixels, which fits the training data well. (h,l) Loss functions. In (a, e, f, g), the red arrow points to a white dot which is captured by the DNN after very long training. We use a DNN with width 500-400-300-200-200-100-100, and learning rate 2×10^{-5} .

follows,

$$y = f(x) = \alpha \times \text{Round}(f_0(x)/\alpha), \quad \alpha \in (0, \infty), \quad (2)$$

where $\text{Round}(\cdot)$ takes the nearest integer value. When $\alpha = 0$, we define $y = f_0(x)$. A feature of this type of functions is that, with the same $f_0(x)$ but different α 's, they share the same dominant low-frequency components.

In a finite interval, e.g., $[-1, 1]$, the frequency components of a target function are quantified by Fourier coefficients computed from DFT. Fig.3a displays the first 40 frequency components of $|F[f](\gamma)|$ for $f_0(x) = x$ and $\alpha = 0.5$ in Eq. (2). Clearly, the dominant first peak of $|F[f_0]|$ and $|F[f]|$ coincide.

Fig.3b shows the Δ_F of the first 40 frequency components at each recording step for $f_0(x) = x$ with $\alpha = 0.5$. It is hard to see what principle the DNN follows when capturing all frequency components. Theoretically, frequency components other than the peaks are susceptible to the artificial periodic boundary

condition implicitly applied in DFT, thereby are not essential to our frequency domain analysis [13]. Therefore, in the following, we only focus on the convergence behavior of the frequency peaks during the training. As shown in Fig. 3c, Δ_F at each frequency peak (marked by black dots in Fig. 3a) converges in a precise order from low- to high-frequency. When we use ReLU as the activation function or use non-uniformly sampled training data for the DNN, we can still see this precise order of convergence of different frequency peaks (Fig. 7 in Appendix 6.1). In the following, we test the validity of F-Principle at different setups and illustrate how it is related to the turning points of information plane trajectory and loss function during the training of DNNs.

We have performed the same frequency domain analysis for various low-frequency dominant functions, such as $f_0(x) = |x|$, $f_0(x) = x^2$ and $f_0(x) = \sin(x)$ with different α 's (data not shown), and F-Principle always holds during the training of DNNs. For illustration, we show another example in Fig. 4a, i.e., $f_0(x) = \sin(x) + 2\sin(3x) + 3\sin(5x)$ with $\alpha = 2$ in Eq. (2), in which the amplitude of low-frequency peaks does not monotonically decrease. In this case, we can still observe a precise convergence order from low- to high-frequency for frequency peaks as shown in Fig. 4b and Fig. 4c. Therefore, F-Principle seems to be an intrinsic behavior of DNN optimization which cannot be explained by the amplitude difference at different frequencies. Note that, for the output of a DNN outside the fitting range, F-Principle also holds by keeping it “flat” (i.e., low frequency dominant) as shown in Fig. 8 in Appendix 6.2.

3.2 Using loss in the Fourier domain to train DNN

As the loss function drives the whole training process of a DNN, one may suspect that it is the difference in driving forces, i.e., the gradients of loss function, at different frequencies that leads to the phenomenon of F-Principle. To investigate this possibility, we rewrite the loss function L_s in Eq. (3) to its frequency domain equivalence L_{wf} in Eq. (4) as follows.

$$L_s = \frac{1}{N} \sum_x (f(x) - T(x))^2, \quad (3)$$

$$L_{wf} = \frac{1}{N} \sum_{\gamma} w(\gamma) |F[f](\gamma) - F[T](\gamma)|^2, \quad (4)$$

where subscripts s and wf respectively denote the spatial domain and the weighted frequency domain. N is the sample size. When $w(\gamma) \equiv 1$ for all frequencies, $L_s = L_{wf}$ according to the Parseval's theorem⁴. This equality gives us a frequency domain decomposition of loss function Eq. (3) as well as its gradient.

⁴ Without loss of generality, the constant factor that is related to the definition of corresponding Fourier Transform is ignored here.

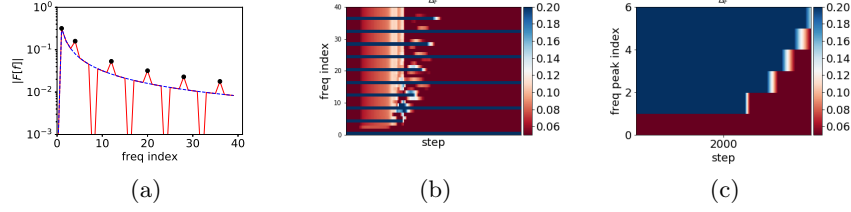


Fig. 3: Frequency domain analysis of the training process of a DNN for $f_0(x) = x$ with $\alpha = 0.5$ in Eq. (2). (a) $|F[f]|$ (red solid line) and $|F[f_0]|$ (blue dashed line) as functions of frequency index. Since the values of all valleys are zero, we use a sufficiently small value of 10^{-4} to replace them for visualization in the log-log scale. Frequency peaks are marked by black dots. (b) Δ_F at different recording steps for different frequency indexes. Δ_F larger than 0.2 (or smaller than 0.05) is represented by blue (or red). (c) Δ_F at different recording steps for different frequency peaks. We use a full-connected tanh-DNN of 4 hidden layers with width: 200-200-200-100. The parameters of the DNN are initialized following a Gaussian distribution with mean 0 and standard deviation 0.1. The activation function for each neuron is tanh. The DNN is trained by full batch Adam optimizer with learning rate 2×10^{-5} . Parameters of the Adam optimizer are set to the default values [8]. The loss function is the mean squared error of the difference between DNN outputs and sample labels in the training set.

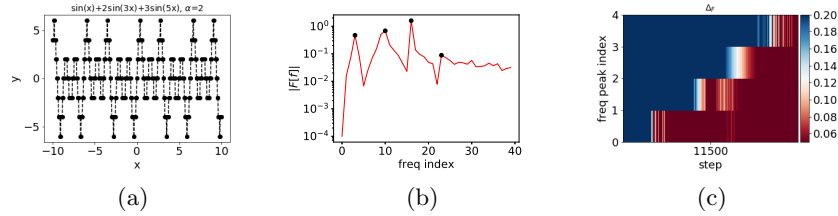


Fig. 4: Frequency domain analysis of the training process of a DNN for $f_0(x) = \sin(x) + 2\sin(3x) + 3\sin(5x)$ with $\alpha = 2$ in Eq. (2). (a) The target function. (b) $|F[f]|$ at different frequency indexes. First four frequency peaks are marked by black dots. (c) Δ_F at different recording steps for different frequency peaks. The training data is evenly sampled in $[-10, 10]$ with sample size 600. DNN settings are the same as the one in Fig. 3.

A natural conjecture would be that the weight $w(\gamma)$ determines the relative speed of convergence towards the target function for each frequency component. However, in Fig.3c, with frequency-wise equally weighted loss function Eq. (3), lower-frequency peaks clearly converge faster than higher-frequency ones. Therefore, we hypothesize that the training process of DNNs implicitly endow lower-frequency components with higher priority by ignoring the higher-frequency components when the lower-frequency components are not well captured. To justify this hypothesis, we can manipulate $w(\gamma)$ so that the weights of higher-frequency components are set to zero at the early stage of training to see if the same convergence behavior as in Fig.3c can be observed.

Specifically, we train DNNs from low- to high-frequency to fit $f_0(x) = x$ with $\alpha = 0.5$ in Eq. (2). Denote $S_p = \{\gamma_i^p | i = 1, 2, \dots, 6\}$, where γ_i^p denotes the frequency index of the i -th frequency peak in Fig.3a. For the i -th frequency peak, we set the weight of the first half part of the frequency domain as $w(\gamma) = 1$ for $0 \leq \gamma \leq \gamma_i^p$, and $w(\gamma) = 0$ for $\gamma > \gamma_i^p$. The second half of weights are fulfilled by the constraint of symmetry. i goes from 1 to 6 in order during the training and is increased by one whenever $\Delta_F(\gamma_i^p) < 10\%$. As shown in Fig.5a, the behavior of Δ_F at different recording steps for different frequency peaks is similar to the one in Fig.3c. This observation conforms with our hypothesis that somehow the higher-frequency components are ignored at the early stage of training.

To further validate our hypothesis, we manually train DNNs from high- to low-frequency to fit the same function of $f_0(x) = x$ with $\alpha = 0.5$ in Eq. (2). For $\gamma_i^p \in S_p$, we set the weight of the first half part of the frequency domain as $w(\gamma) = 0$ for $0 \leq \gamma < \gamma_i^p$, and $w(\gamma) = 1$ for $\gamma \geq \gamma_i^p$. The second half of weights are fulfilled by the constraint of symmetry. i goes from 6 to 1 in order during the training and is decreased by one whenever $\Delta_F(\gamma_i^p) < 10\%$ or the number of recording steps used for fitting the i -th peak reaches 5000. We add the latter condition because the convergence speed for high-frequency components in this approach is often very slow. Fig.5b shows that $\Delta_F(\gamma_i^p)$ starts to converge properly only when all frequency components are used for training after recording step 17000. This observation further justifies our hypothesis that higher-frequency components indeed have lower priority as they converge efficiently and properly only when the lower-frequency components are well captured. Therefore, F-Principle is an intrinsic behavior of the DNN optimization process, which implicitly endows lower-frequency components with higher priority.

4 F-Principle in understanding DNN

In this section, we focus on how F-Principle can be used to understand the generalization of DNN. Why DNNs capable of over-fitting often generalize well is a mystery in deep learning [7,11,21,20,10,17]. By F-Principle, this mystery could be naturally explained as follows. For a class of functions dominated by low frequencies, with finite training data points, there is an *effective frequency range* for this training set, which is defined as the range in frequency domain

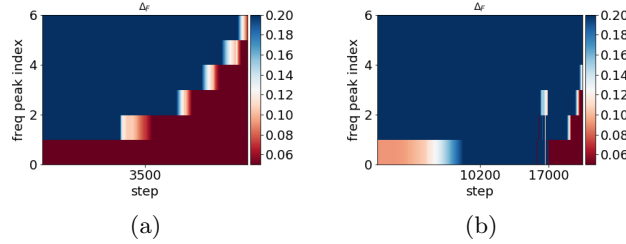


Fig. 5: Analysis of DNN training process with loss function L_{wf} for $f_0(x) = x$ with $\alpha = 0.5$ in Eq. (2). (a) Δ_F at different recording steps for different frequency peaks using L_{wf} with $w(\gamma)$ tuned from low- to high-frequency. (b) Δ_F at different recording steps for different frequency peaks using L_{wf} with $w(\gamma)$ tuned from high- to low-frequency. DNN settings are the same as the one in Fig. 3.

bounded by Nyquist-Shannon sampling theorem [15] when the sampling is evenly spaced, or its extensions [19,12] otherwise. When the number of parameters of a DNN is greater than the size of the training set, the DNN can over-fit these sampling data points (i.e., training set) with different amount of powers outside the effective frequency range. However, by F-Principle, the training process will implicitly bias the DNN towards a solution with low power for the high-frequency components outside the effective frequency range. For functions dominated by low frequencies, this bias coincides with their intrinsic feature of low power at high frequencies, thus naturally leading to a well-generalized solution after training. By the above analysis, we can predict that, in the case of insufficient training data, when the higher-frequency components are not negligible, e.g., there exists a significant frequency peak above the effective frequency range, the DNN cannot generalize well after training.

In another case where the training data is contaminated by noise, early-stopping method is usually applied to avoid overfitting in practice [10]. By F-Principle, early-stopping can help avoid fitting the noisy high-frequency components. Thus, it naturally leads to a well-generalized solution which accurately captures the dominant low-frequency components while keeping the high-frequency ones small. We use the following example for illustration.

As shown in Fig.6a, we consider $f_0(x) = \sin(x)$ with $\alpha = 0.5$ in Eq. (2). For each sample x , we add a noise ϵ on $f_0(x)$, where ϵ follows a Gaussian distribution with mean 0 and standard deviation 0.1. The training set and the test set respectively consist of 300 and 6000 data points evenly sampled in $[-10, 10]$. The DNN can well fit the sampled training set as the loss function of the training set decreases to a very small value (green stars in Fig.6b). However, the loss function of the test set first decreases and then increases (red dots in Fig.6b). That is, the generalization performance of the DNN gets worse during the training after a certain step. In Fig.6c, $|F[f]|$ for the training data (red) and the test data (black) only overlap around the dominant low-frequency components. This

indicates that the noise in samples has much more impact on high-frequency components. Around step 296 (green dashed lines in Fig. 6b and d), the DNN well captures the dominant peak as shown in Fig. 6c, and the loss function of the test set attains its minimum and starts to increase (red dots in Fig.6b). These phenomena are consistent with our above analysis that early-stopping helps prevent fitting the noisy high-frequency components thus naturally leads to a better generalization performance of DNNs.

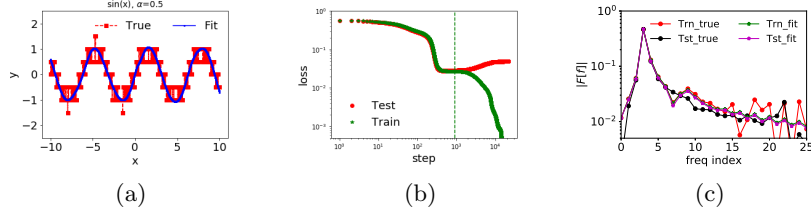


Fig. 6: Frequency domain analysis of the training process of the DNN for a dataset contaminated by noise. In this example, $f_0(x) = \sin(x)$ with $\alpha = 0.5$ in Eq. (2). For each sample at x , we add a noise ϵ on $f_0(x)$, where ϵ follows a Gaussian distribution with mean 0 and standard deviation 0.1. The training set and the test set respectively consist of 300 and 6000 data points evenly sampled in $[-10, 10]$. (a) The sampled values of the test set (red square dashed line) and DNN outputs at recording step 296 (blue solid line). (b) Loss functions for training set (green stars) and test set (red dots) at different recording steps. The green dashed lines are drawn at step 296, around where the best generalization performance is achieved. (c) $|F[f]|$ for the training set (red) and test set (black), and $|F[T]|$ for the training set (green), and test set (magenta) at recording step 296. DNN settings are the same as the one in Fig. 3.

5 Discussion and conclusion

In this work, we empirically found a widely applied principle, i.e., F-Principle, underlying the optimization process of DNNs for fitting 1-d functions, memorizing natural images, and classification problems. Specifically, for a function with dominant low-frequency components, DNNs with common settings first capture these low-frequency components while keeping high-frequency ones small. In our experiments, this phenomenon can be widely observed for DNNs with different neuron numbers (tens to thousands in each layer), layer numbers (one to tens), training algorithms (GD, SGD, Adam), and activation functions (tanh and ReLU). From our analysis, F-Principle is an intrinsic property of DNN optimization process under common settings. It can well explain the good generalization

performance of DNNs often observed in experiments. In Appendix 6.3, we also discuss how to use the F-Principle to understand the behavior of the training process in the information plane. Our findings could potentially provide insights into the behavior of DNN optimization process in general.

Note that initializing weights with large values could complicate the phenomenon of F-Principle. In previous experiments, most DNNs are initialized by Gaussian distribution with mean 0 and small standard deviation, and its training behavior follows F-Principle. However, with large-initialization values, F-Principle can fail (see Fig.2d). More importantly, although the DNN can well fit the training data for both initializations, these two initializations could result in very different generalization performances, that is, good generalization for the small initialization in Fig.2h and bad generalization for the large initialization in Fig.2l. Intuitively, the above phenomenon can be understood as follows. For the large initialization, the initial output of the DNN is very fluctuated, that is, some high-frequency components are large at the initial output (Fig.2i). Without explicit constraints on the high-frequency components beyond the effective frequency range of the training data, the DNN output after training tends to inherit these high-frequency components from the initial output. Therefore, with large-initialization values, DNN outputs can easily overfit the target function with fluctuating high-frequency components. In practice, the weights of DNNs are often randomly initialized with standard deviations close to zero [17]. As suggested by our analysis, the small-initialization strategy may implicitly lead to a more efficient and well-generalized optimization process of DNNs as characterized by F-Principle.

Acknowledgments

The authors want to thank David W. McLaughlin for helpful discussions and thank Qiu Yang, Zheng Ma, and Tao Luo for critically reading the manuscript. ZX, YZ, YX are supported by the NYU Abu Dhabi Institute G1301. The authors declare no conflict of interest.

6 Appendix

6.1 Examples of F-Principle

For illustration, Fig.7 shows that F-Principle holds when we use ReLU as the activation function (see Fig.7a) or use non-uniformly sampled training data (see Fig.7b) for DNNs.

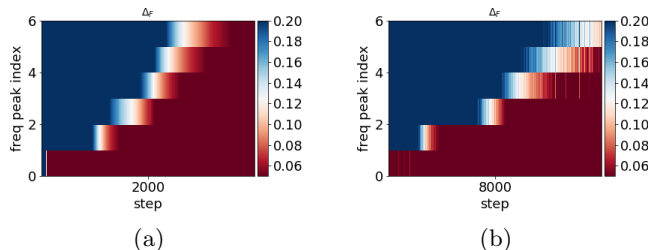


Fig.7: Δ_F at different recording steps for different frequency peaks as shown in Fig. 3a under different settings. (a) ReLU is used as activation function. (b) Training data is sampled non-uniformly as follows. We first evenly sample 3000 points in $[-1, 1]$. Then, the training data is sampled randomly from these 3000 data points with sample size 600. Note that, for the non-uniform sampling example, we use hidden layers with width 400-400-400-200-200 to accelerate the training process. All other DNN settings are the same as Fig.3.

6.2 DNN outputs outside the fitting range

We observe in our experiments that, outside the fitting range of the training data, the DNN output is very flat. For illustration, we train a DNN to fit an oscillation function $f(x) = \sin(x)$. At the end of training, the DNN well captures the fitting range $[-10, 10]$, whereas, outside the fitting range, it is very flat with no oscillation, as shown in Fig.8. This indicates that, without constraints outside the fitting range, the DNN keeps its output low-frequency (close to 0) dominant.

6.3 Compression vs. no compression in the information plane

Through the empirical exploration of DNN training in the information plane, regarding information compression phase, Schwartz-Ziv and Tishby (2017) [16] claimed that (i) information compression is a general process; (ii) information

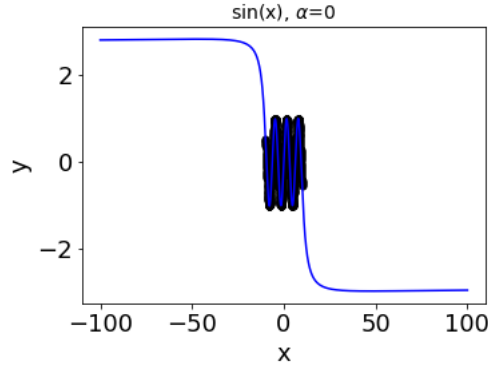


Fig. 8: DNN output after training (blue line) for $f(x) = \sin(x)$. Black dots indicate training data, which is evenly sampled in $[-10, 10]$ with sample size 600.

compression is induced by SGD. In this sub-section, we demonstrate how F-Principle can be used to understand when the compression phase can appear in the information plane. Note that a detailed discussion of mutual information can be found in Appendix 6.4.

We first demonstrate how compression can appear or disappear by tuning a parameter in Eq. (2) with $f_0(x) = x$ for $x \in [-1, 1]$ using full batch gradient descent (GD) without stochasticity. In our simulations, the DNN well fits $f(x)$ for both α equal to 0 and 0.5 after training (see Fig.9a and c). In the information plane, there is no compression phase for $I(T)$ for $\alpha = 0$ (see Fig.9b). By increasing α in Eq. (2) we can observe that: i) the fitting function is discretized with only few possible outputs (see Fig.9c); ii) the compression of $I(T)$ appears (see Fig.9d). For $\alpha > 0$, behaviors of information plane are similar to previous results [16]. To understand why compression would happen for $\alpha > 0$, we next focus on the training courses for different α in the frequency domain.

A key feature of the class of functions in Eq. (2) is that the dominant low-frequency components for $f(x)$ with different α are the same (see Fig.3a). By F-Principle, the DNN first capture those dominant low-frequency components, thus, the training courses for different α at the beginning are similar, i.e., i) the DNN output is close to $f_0(x)$ at certain training epochs (blue lines in Fig.9a and c); ii) $I(T)$ in the information plane increases rapidly until it reaches a value close to the entropy of $f_0(x)$, i.e., $I(f_0(x))$ (see Fig.9b and d). For $\alpha = 0$, the target function is $f_0(x)$, therefore, $I(T)$ would be closer and closer to $I(f_0(x))$ during the training. For $\alpha > 0$, the entropy of the target function, $I(f(x))$, is much less than $I(f_0(x))$. In the latter stage of capturing high-frequency components, the DNN output T would converge to the discretized function $f(x)$. Therefore, $I(T)$ would decrease from $I(f_0(x))$ to $I(f(x))$.

Actually, for $f(x) = x$, theoretically, $I(Y) \geq I(Y, T) = I(X, T) = I(T)$ and $I(T)$ would finally converge to $I(Y)$. Thus, $f(x) = x$ is a trivial case that

compression phase could not occur. This analysis is also applicable for other continuous functions. For any discretized function, the DNN first fits the low-frequency components of the discretized function with a continuous function. Then, the DNN output converges to discretized values as the network gradually captures the high-frequency components. By the definition of entropy, this discretization process naturally reduces the entropy of the DNN output. Thus, the compression phase appears in the information plane. As the discretization in general is inevitable for classification problems with discrete labels, we can often observe information compression in practice as described in the previous study [16].

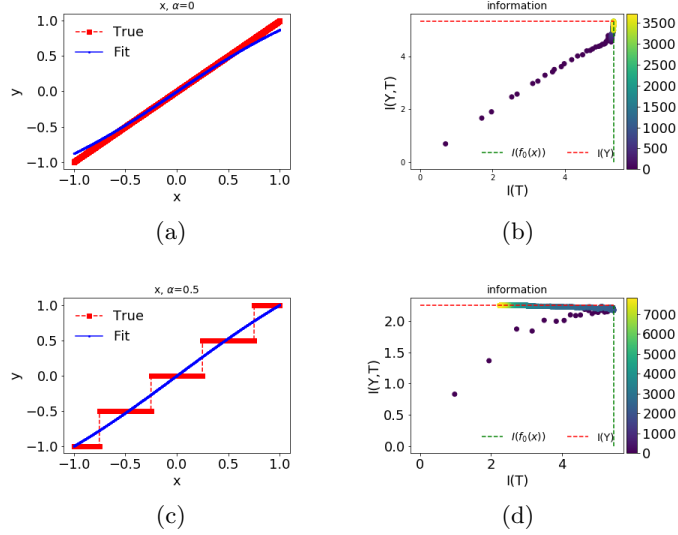


Fig. 9: Analysis of compression phase in the information plane. α is 0 for (a, b) and 0.5 for (c, d). (a, c) $f(x)$ (red square) with $f_0(x) = x$ in Eq. (2) and the DNN output (blue solid line) at step $R_c(\gamma_1^P, 5\%)$. (b, d) Trajectories of the training process of the DNN in the information plane. Color of each dot indicates its recording step. The green dashed vertical line and the red dashed horizontal line indicate constant values of $I(f_0(x))$ and $I(Y)$, respectively.

6.4 Computation of information

For any random variables U and V with a joint distribution $P(u, v)$: the entropy of U is defined as $I(U) = -\sum_u P(u) \log P(u)$; their mutual information is defined as $I(U, V) = \sum_{u,v} P(u, v) \log \frac{P(u, v)}{P(u)P(v)}$; the conditional entropy of U on V

is defined as

$$I(U|V) = \sum_{u,v} P(u,v) \log \frac{P(v)}{P(u,v)} = I(U) - I(U,V).$$

By the construction of the DNN, its output T is a deterministic function of its input X , thus, $I(T|X) = 0$ and $I(X,T) = I(T)$. To compute entropy numerically, we evenly bin X, Y, T to X_b, Y_b, T_b with bin size b as follows. For any value v , its binned value is define as $v_b = \text{Round}(v/b) \times b$. In our work, $I(T)$ and $I(Y,T)$ are approximated by $I(T_b)$ and $I(Y_b, T_b)$, respectively, with $b = 0.05$. Note that, after binning, one value of X_b may map to multiple values of T_b . Thus, $I(T_b|X_b) \neq 0$ and $I(X_b, T_b) \neq I(T_b)$. The difference vanishes as bin size shrinks. Therefore, with a small bin size, $I(T_b)$ is a good approximation of $I(X,T)$. In experiments, we also empirically found that $I(X_b, T_b)$ and $I(T_b)$ behave almost the same in the information plane for the default value $b = 0.05$ (data not shown).

References

1. Alain, G., Bengio, Y.: Understanding intermediate layers using linear classifier probes. arXiv preprint arXiv:1610.01644 (2016)
2. Arpit, D., Jastrzebski, S., Ballas, N., Krueger, D., Bengio, E., Kanwal, M.S., Maharaj, T., Fischer, A., Courville, A., Bengio, Y., et al.: A closer look at memorization in deep networks. arXiv preprint arXiv:1706.05394 (2017)
3. Barnett, A., Greengard, L., Pataki, A., Spivak, M.: Rapid solution of the cryo-em reconstruction problem by frequency marching. *SIAM Journal on Imaging Sciences* 10(3), 1170–1195 (2017)
4. Dong, D.W., Atick, J.J.: Statistics of natural time-varying images. *Network: Computation in Neural Systems* 6(3), 345–358 (1995)
5. Hackbusch, W.: Multi-grid methods and applications, vol. 4. Springer Science and Business Media (2013)
6. Hardt, M., Recht, B., Singer, Y.: Train faster, generalize better: Stability of stochastic gradient descent. arXiv preprint arXiv:1509.01240 (2015)
7. Kawaguchi, K., Kaelbling, L.P., Bengio, Y.: Generalization in deep learning. arXiv preprint arXiv:1710.05468 (2017)
8. Kingma, D.P., Ba, J.: Adam: A method for stochastic optimization. arXiv preprint arXiv:1412.6980 (2014)
9. LeCun, Y., Bengio, Y., Hinton, G.: Deep learning. *nature* 521(7553), 436 (2015)
10. Lin, J., Camoriano, R., Rosasco, L.: Generalization properties and implicit regularization for multiple passes sgm. In: International Conference on Machine Learning. pp. 2340–2348 (2016)

11. Martin, C.H., Mahoney, M.W.: Rethinking generalization requires revisiting old ideas: statistical mechanics approaches and complex learning behavior. arXiv preprint arXiv:1710.09553 (2017)
12. Mishali, M., Eldar, Y.C.: Blind multiband signal reconstruction: Compressed sensing for analog signals. *IEEE Transactions on Signal Processing* 57(3), 993–1009 (2009)
13. Percival, D.B., Walden, A.T.: Spectral analysis for physical applications. cambridge university press (1993)
14. Saxe, A.M., Bansal, Y., Dapello, J., Advani, M.: On the information bottleneck theory of deep learning. *International Conference on Learning Representations* (2018)
15. Shannon, C.E.: Communication in the presence of noise. *Proceedings of the IRE* 37(1), 10–21 (1949)
16. Shwartz-Ziv, R., Tishby, N.: Opening the black box of deep neural networks via information. arXiv preprint arXiv:1703.00810 (2017)
17. Wu, L., Zhu, Z., E, W.: Towards understanding generalization of deep learning: Perspective of loss landscapes. arXiv preprint arXiv:1706.10239 (2017)
18. Xu, Z.J.: Understanding training and generalization in deep learning by fourier analysis. arXiv preprint arXiv:1808.04295 (2018)
19. Yen, J.: On nonuniform sampling of bandwidth-limited signals. *IRE Transactions on circuit theory* 3(4), 251–257 (1956)
20. Zhang, C., Bengio, S., Hardt, M., Recht, B., Vinyals, O.: Understanding deep learning requires rethinking generalization. arXiv preprint arXiv:1611.03530 (2016)
21. Zheng, G., Sang, J., Xu, C.: Understanding deep learning generalization by maximum entropy. arXiv preprint arXiv:1711.07758 (2017)